

Nonlinear dynamic analysis of fractional order rub-impact rotor system

Junyi Cao^{a,*}, Chengbin Ma^b, Zhuangde Jiang^a, Shuguang Liu^c

^a State Key Laboratory for Manufacturing Systems Engineering, Research Institute of Diagnostics and Cybernetics, Xi'an Jiaotong University, Xi'an 710049, China

^b UM-SJTU Joint Institute, Shanghai Jiaotong University, Shanghai 200240, China

^c Xian Polytechnic University, Xi'an 710048, China

ARTICLE INFO

Article history:

Received 6 August 2009

Received in revised form 2 July 2010

Accepted 3 July 2010

Available online 17 July 2010

Keywords:

Fractional calculus

Rub-impact

Nonlinear dynamics

Rotor-bearing system

ABSTRACT

Nonlinear dynamic characteristics of rub-impact rotor system with fractional order damping are investigated. The model of rub-impact comprises a radial elastic force and a tangential Coulomb friction force. The fractional order damped rotor system with rubbing malfunction is established. The four order Runge–Kutta method and ten order CFE-Euler method are introduced to simulate the fractional order rub-impact rotor system equations. The effects of the rotating speed ratio, derivative order of damping and mass eccentricity on the system dynamics are investigated using rotor trajectory diagrams, bifurcation diagrams and Poincare map. Various complicated dynamic behaviors and types of routes to chaos are found, including period doubling bifurcation, sudden transition and quasi-periodic from periodic motion to chaos. The analysis results show that the fractional order rub-impact rotor system exhibits rich dynamic behaviors, and that the significant effect of fractional order will contribute to comprehensive understanding of nonlinear dynamics of rub-impact rotor.

© 2010 Elsevier B.V. All rights reserved.

1. Introduction

Since fractional calculus has a profound impact on many engineering and scientific areas such as automatic control, signal and image processing, bioengineering, electrochemistry, mechanics, viscoelasticity and rheology, the applications of fractional calculus in engineering and physics have become a recent focus of research internationally [1,2]. Especially the dynamics and vibration analysis of fractional order damped systems are of great interest to researchers [3–9]. The fractional order operator's characteristic of having an unlimited memory leads to a concise description of complicated system dynamics. For example, the backlash and impact can be more adequately analyzed [10,11]. Ge et al. introduce the chaos control of the fractional order rotational mechanical system [12]. Machado et al. also argue that while the dynamics of each individual element has an integer-order nature, the global dynamics reveals the existence of both integer and fractional order nature [13]. Therefore, it is essential to consider the fractional order damping in studying the dynamic characteristics.

Nonlinear dynamic analysis of rotor-bearing system is of great significance to exactly diagnose the malfunctions and improve the dynamic characteristics of a rotor system effectively. Therefore a number of articles on this topic have been published to analyze the nonlinear dynamics of rub-impact rotor.

Muszynska surveys the publications on rub phenomena up to then and discussed the major physical phenomena that occur during rubbing [14]. Beatty proposes a mathematical model for rubbing forces which is still widely used and he concluded some important points for diagnosing this fault [15]. Chu and Zhang analyze the bifurcation and chaotic motion of a rub-impact rotor system, three different routes to chaos along with the increasing rotating speed are found [16]. Later,

* Corresponding author.

E-mail address: caojy@mail.xjtu.edu.cn (J. Cao).

Chu observes very rich forms of periodic and chaotic vibrations through experimental verification. These results are of importance to the fault diagnosis of the rub-impact problem [17]. Ehrich studies about the bifurcation of a bearing-rotor system identifying a sub-harmonic vibration phenomenon in a rotor dynamic system [18]. Goldman and Muszynska analyze the chaotic behavior of rub-impact rotor using numerical emulation and simple experimental verification, they conclude that the rub can lead to higher order harmonic, sub-harmonic fractional frequency, or to chaotic vibrations [19]. Lin et al. analyze the nonlinear behavior of rub-related vibration in rotating machinery. The effects of rotating speed, clearance, damping factor, friction coefficient, and boundary stiffness are investigated [20]. Feng and Zhang discuss the vibration phenomena of a rotor rubbing with a stator caused by an initial perturbation. They find that in the case of no friction between the rotor and the stator, the full rubbing behaves as forward whirling and when the friction was present the full rubbing behaves as backward whirling [21]. Choi argues the nonlinear model of rotor system when partial rub occur and finds the typical nonlinear phenomena of partial rub through the estimated nonlinear model and experiments [22]. Chang-jian et al. analyze nonlinear dynamic of rub-impact rotor supported by turbulent journal bearings with nonlinear suspension [23]. Qin et al. discuss the nonlinear vibration responses of a rub-impact overhung rotor based on the transfer matrix method and observe the rich nonlinear dynamics induced by the variation of rotating speed, imbalance and external damping [24]. Shen et al. investigate the vibration characteristics of a rub-impact rotor-bearing system excited by mass unbalance [25], while Patel and Darpe examine vibration response of the cracked rotor in presence of rotor stator rub [26].

Based on the above analysis, we found that the rub-impact rotor system has very complicated spectrum characteristics and can exhibit very rich form of periodic, quasi-periodic and chaotic vibrations. Moreover, the effects of rotating speed, clearance, damping factor, friction coefficient, and mass unbalance are discussed. However, most of the previous researches are based on integer-order damping and the nonlinear dynamics of a rub-impact rotor-bearing system with fractional order damping has rarely been investigated. Therefore, the present work analyzes the dynamic behavior of rub-impact rotor with fractional order damping. The analysis focuses on the effects of fractional order damping, rotating speed and mass eccentricity. For simplicity, the Jeffcott rotor is taken into account in the dynamic analysis and the rubbing forces are supposed to consist of a radial elastic force and a tangential Coulomb friction force. The ten order direct approximation using Euler rule and Continued Fraction Expansion is introduced for numerical simulation of rub-impact rotor system with fractional order damping. Dynamic trajectory, power spectrum, Poincare map, bifurcation diagram are applied to analyze the dynamic response.

2. Fractional calculus and approximation schemes

The two definitions for fractional differentiation and integration are the Grunwald–Letnikov (GL) definition and the Riemann–Liouville (RL) definition [27]. The GL definition is the best known one since it is most direct for the digital realization of the fractional order operators. The GL fractional derivative of continuous function $f(t)$ is given by:

$${}_a D_t^\alpha f(t) = \lim_{h \rightarrow 0} h^{-\alpha} \sum_{j=0}^{\lfloor \frac{t-a}{h} \rfloor} (-1)^j \binom{\alpha}{j} f(t-jh) \quad (1)$$

where $[\cdot]$ is a truncation, $\binom{\alpha}{j}$ is binomial coefficients, it can be replaced by the Gamma function, $\binom{\alpha}{j} = \frac{\Gamma(\alpha+1)}{j! \Gamma(\alpha-j+1)}$, while the RL definition is given by:

$${}_a D_t^\alpha f(t) = \frac{1}{\Gamma(n-\alpha)} \frac{d^n}{dt^n} \int_a^t \frac{f(\tau)}{(t-\tau)^{\alpha-n+1}} d(\tau) \quad (2)$$

for $(n-1 < \alpha < n)$

Fractional order calculus is quite complicated in time domain, as shown in the above two definitions. However, it is usually more easily to describe in Laplace domain. The Laplace transform of the fractional integral of $f(t)$ is given by:

$$L\{{}_0 D_t^\alpha f(t)\} = s^\alpha F(s) \quad (3)$$

where $F(s)$ is the Laplace transform of $f(t)$. The Laplace transform of the fractional derivative of $f(t)$ is given as follows:

$$L\{{}_0 D_t^\alpha f(t)\} = s^\alpha F(s) - \sum_{k=1}^{n-1} s^k [{}_0 D_t^{\alpha-k-1} f(0)] \quad (4)$$

where $n-1 < \alpha < n$ again. If all the initial conditions are zeros, the Laplace transform of fractional derivative is simplified to Eq. (3). It can be viewed From Eq. (3) that the numerical computation of the fractional order operators s^α is important to solve the fractional derivative equation.

In order to exactly realize the fractional order operators, all the past inputs need to be memorized, which is not impossible in real applications. There are mainly two discretization methods for the approximation of the operators s^α , direct discretization and indirect discretization [28]. Various direct discretization methods have been proposed, such as short memory principle, sampling time scaling and the expansion of various operators such as Tustin, Al-Alaoui and Euler operators by Power Series Expansion (PSE) or Continued Fraction Expansion (CFE) [29–31]. For the PSE method, the differential equations

are in FIR filter structure; while the approximation equations for the CFE method are in IIR filter structure. The following explanation is to adopt Euler operator for direct discretization of the fractional order operator, which can be given by:

$$s^\alpha = \left(\frac{1 - z^{-1}}{T}\right)^\alpha \tag{5}$$

Then perform CFE, the discretization result is as follows:

$$Z\{D^\alpha x(t)\} = CFE\left\{\left(\frac{1 - z^{-1}}{T}\right)^\alpha\right\}X(z) \approx \left(\frac{1}{T}\right)^\alpha \frac{P_p(z^{-1})}{Q_q(z^{-1})}X(z). \tag{6}$$

where $CFE\{u\}$ denotes the Continued Fraction Expansion of u ; p and q are the orders of the approximation; P and Q are polynomials of degrees p and q . Usually p , q and n can be set to be equal, $p = q = n$. In the below numerical analysis, the order of the approximation equation is chosen as 10.

3. Mathematical modeling

The rub-impact model based on Jeffcott rotor system is derived by Chu and Zhang [16]. Supposing the center of the stator to be the origin of the coordinates, Displacements of the disk center (x, y) , the mass eccentricity of this disk e_M , and the rub-impact forces (F_x, F_y) , the system equations of motion can be described as follows:

$$\begin{cases} M \frac{d^2x}{dt^2} + c \frac{dx}{dt} + kx = Me_M\omega^2 \cos \omega t + F_x \\ M \frac{d^2y}{dt^2} + c \frac{dy}{dt} + ky = Me_M\omega^2 \sin \omega t + F_y - Mg \end{cases} \tag{7}$$

where c is the damping coefficient of the shaft, k is the stiffness coefficient of the shaft, ω is the rotating speed.

The damping model using fractional derivative has many successful applications in the mechanical engineering [32–34], because it can exhibit the complicated frequency dependency of damping materials. The fractional order damping force using fractional calculus is:

$$F_d = cD^\alpha x(t) \tag{8}$$

where α is fractional and derivative order of damping. When the fractional order damping is taken into account in dynamic analysis of rub-impact rotor, the system motion equation can be changed as:

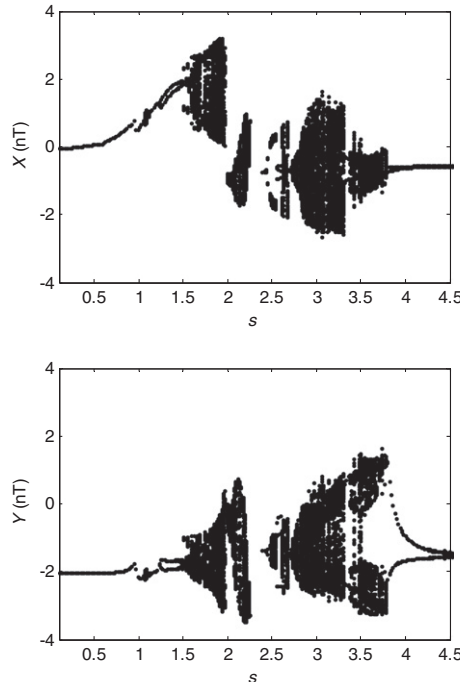


Fig. 1. Bifurcation diagrams of X and Y versus s for $TS = 2\pi/500$ and $\alpha = 0.5$.

$$\begin{cases} M \frac{d^2x}{dt^2} + cD^\alpha x + kx = Me_M \omega^2 \cos \omega t + F_x \\ M \frac{d^2y}{dt^2} + cD^\alpha y + ky = Me_M \omega^2 \sin \omega t + F_y - Mg \end{cases} \quad (9)$$

The rotor rub-impact force model used in this paper is proposed by Beatty [15], It is assumed that there is an initial clearance of δ between rotor and stator, the radial force from impact is elastic and the tangential friction force satisfies the Coulomb type of frictional relationship. When the rubbing happens, the radial impact force F_N and the tangential rub force F_T can thus be written as

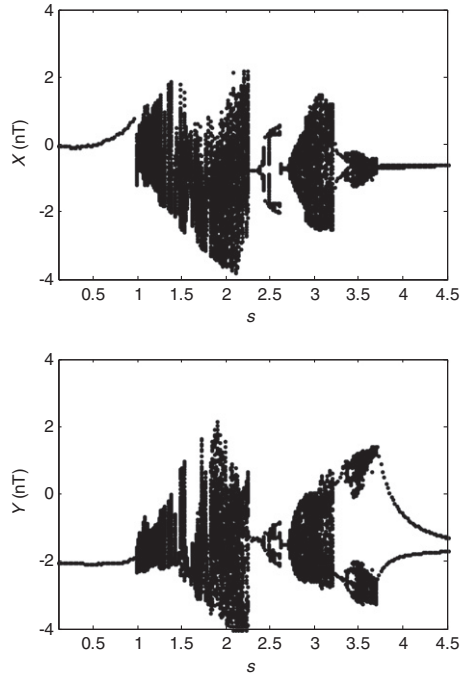


Fig. 2. Bifurcation diagrams of X and Y versus s for TS = 2pi/300 and $\alpha = 0.5$

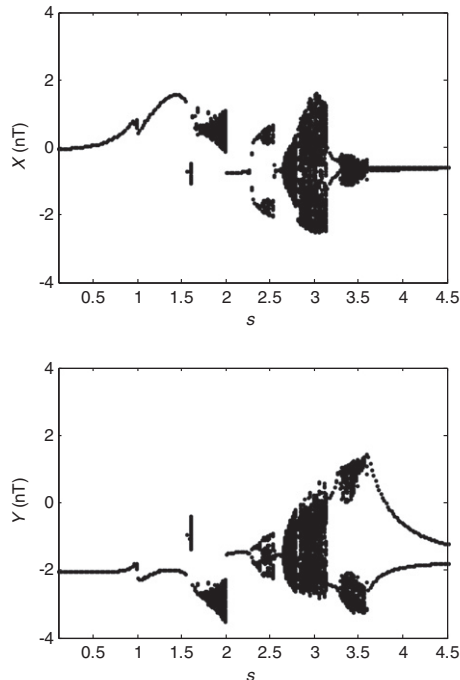


Fig. 3. Bifurcation diagrams of X and Y versus s for TS = 2pi/500 and $\alpha = 1.0$.

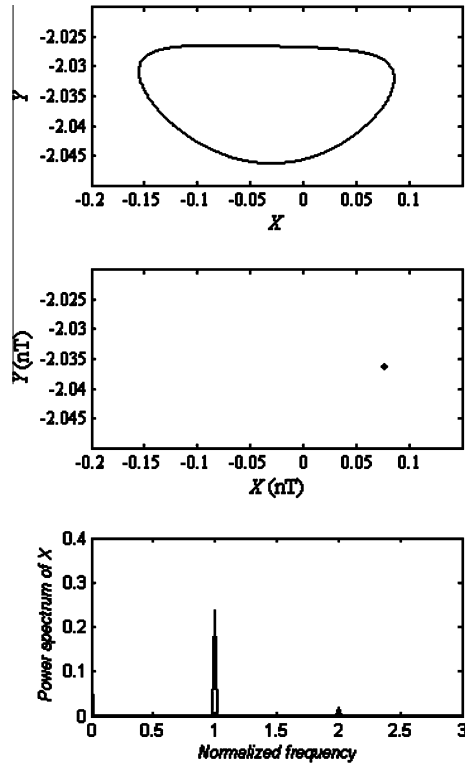


Fig. 4. Phase trajectory, Poincaré map and power spectrum for $s = 0.5$.

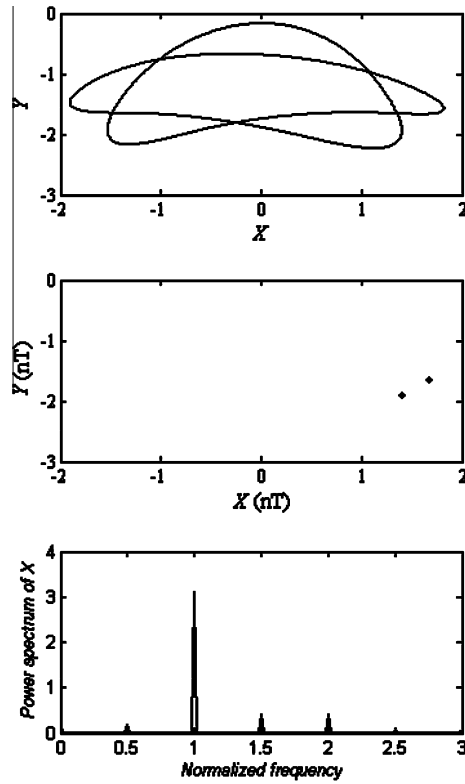


Fig. 5. Phase trajectory, Poincaré map and power spectrum for $s = 1.3$.

$$F_N = \begin{cases} 0 & (r < \delta) \\ (r - \delta)k_c & (r \geq \delta) \end{cases}, \quad F_T = fF_N \tag{10}$$

where k_c is radial stiffness of the stator. f is the friction coefficient between the stator and the rotor. $r = \sqrt{x^2 + y^2}$ is the radial displacement of the rotor. In the $x - y$ coordinate system, these two forces can be rewritten as:

$$\begin{cases} \begin{pmatrix} F_x \\ F_y \end{pmatrix} = -\frac{r-\delta}{r}k_c \begin{bmatrix} 1 & -f \\ f & 1 \end{bmatrix} \begin{pmatrix} x \\ y \end{pmatrix} & (r \geq \delta) \\ F_x = F_y = 0 & (r < \delta) \end{cases} \tag{11}$$

It is clearly indicated in this equation that when $r < \delta$, there will be no rub-impact interaction and the rub-impact forces are zero while the rub-impacting will happen if $r \geq \delta$.

Taking the nonlinear rub-impact forces and fractional order damping into account, the system governing equation of rub-impact rotor can be simplified by the non-dimensional parameter. The non-dimensional parameters are introduced as follows:

$$X = \frac{x}{\delta}, \quad Y = \frac{y}{\delta}, \quad T = \omega t, \quad \zeta = \frac{c}{2\sqrt{k \times M}}, \quad s = \frac{\omega}{\omega_n}, \quad \omega_n = \sqrt{k/M}$$

$$\frac{d}{dt} = \omega \frac{d}{dT}, \quad \frac{d^2}{dt^2} = \omega^2 \frac{d^2}{dT^2}, \quad \beta = \frac{e_M}{\delta}$$

where X and Y are the non-dimensional displacements of the disk center, T is the non-dimensional time, ζ is the damping ratio referred to the critical damping of a linear system with the larger stiffness k , s is the rotational speed ratio, ω_n is the natural frequency of the linear stiff system. The non-dimensional governing equations are as follows:

$$\begin{cases} \frac{d^2X}{dT^2} + \frac{2\zeta}{s}D^\alpha X + \frac{1}{s^2}X = \beta \cos T + \frac{F_x}{M\omega^2\delta} \\ \frac{d^2Y}{dT^2} + \frac{2\zeta}{s}D^\alpha Y + \frac{1}{s^2}Y = \beta \sin T + \frac{F_y}{M\omega^2\delta} - \frac{g}{\omega^2\delta} \end{cases} \tag{12}$$

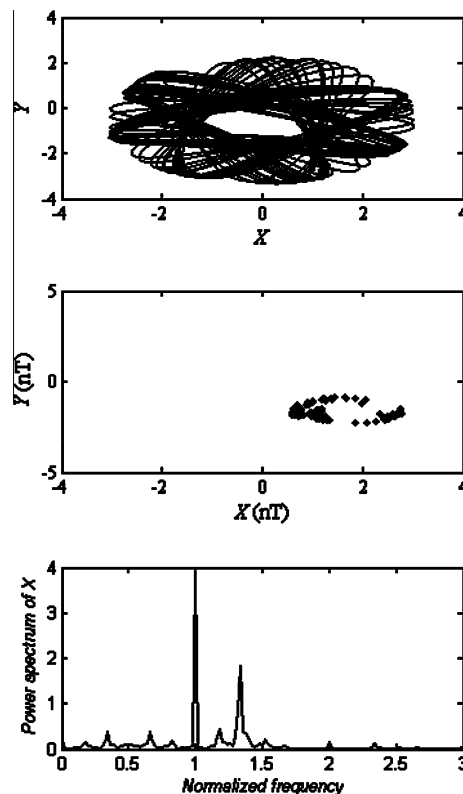


Fig. 6. Phase trajectory, Poincaré map and power spectrum for $s = 1.68$.

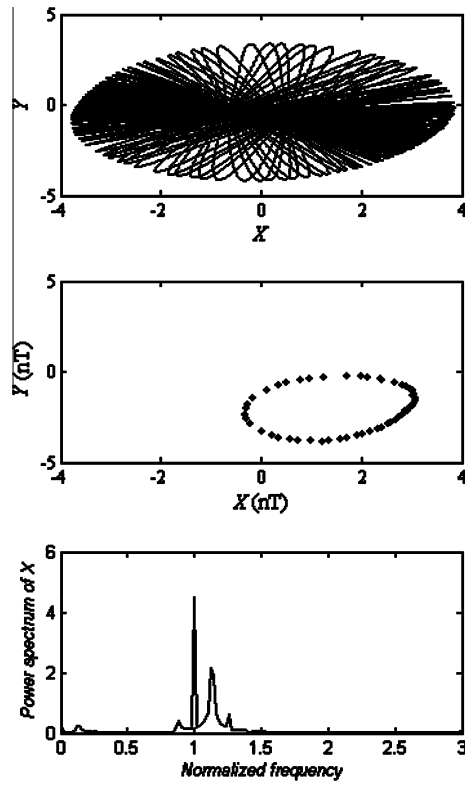


Fig. 7. Phase trajectory, Poincaré map and power spectrum for $s = 2.1$.

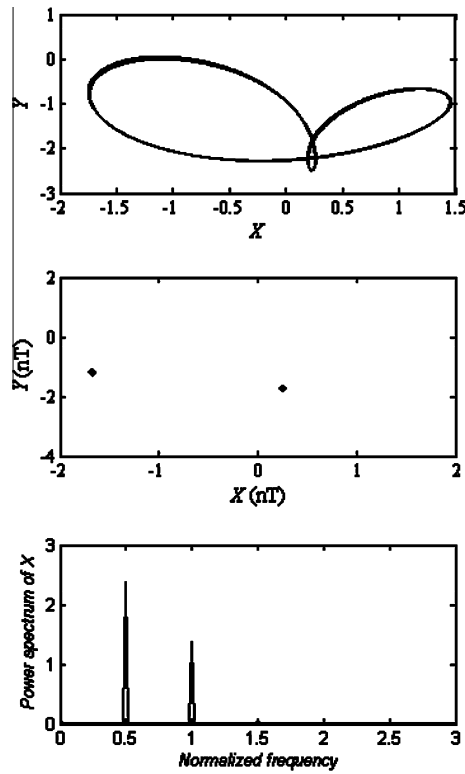


Fig. 8. Phase trajectory, Poincaré map and power spectrum for $s = 2.45$.

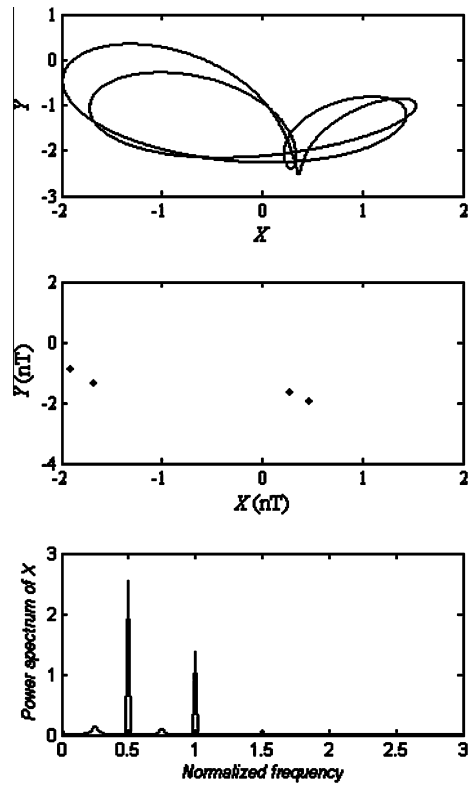


Fig. 9. Phase trajectory, Poincaré map and power spectrum for $s = 2.53$.

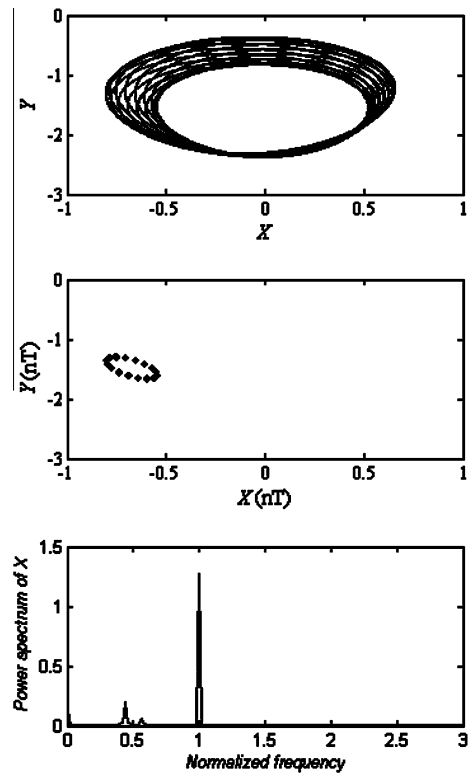


Fig. 10. Phase trajectory, Poincaré map and power spectrum for $s = 2.7$.

4. Results and discussions

The nonlinear dynamics of rub-impact rotor with fractional damping is digitally simulated in Matlab/Simulink. The fractional derivative of Eq. (12) is approximated by IIR discrete model employing CFE and Euler rule, in which the order of approximation model is equal to 10. The four order Runge–Kutta method is used to solve the system non-dimensional governing equations. One of the key parameters for numerical analysis is the time step (TS), the bifurcation diagrams for $TS = 2\pi/500$ and $TS = 2\pi/300$ are showed in Figs. 1 and 2, respectively. Because lower time step can provide the exact results and capture the transient dynamic behaviors, The time step used here is set to $2\pi/500$. The stable response value can be obtained through discarding the output of former 50 periods and remaining the output of last 100 periods. That is to say, the response output in diagrams should be considered as stable state output. Therefore, a large number of computations are required, and the number of data points plotted in dynamic orbit diagrams is 50,000. In the numerical analysis, the system parameters are specified as: $M = 30$ kg, $k = 5.6 \times 10^5$ N/m, $k_c = 6.5 \times 10^6$ N/m, $c = 1100$ Ns/m, $\delta = 0.2$ mm, $e_M = 0.1$ mm, $g = 9.8$ N/kg. The initial state is set to $X(0) = 0, Y(0) = 0$.

4.1. Influence of speed

The rotational velocity is one of the key parameters affecting the dynamic behavior of rotor-bearing system. When $\alpha = 0.5$, the bifurcation diagram obtained by using the rotational speed ratio as the control parameter is shown in Fig. 1. In case of $\alpha = 1.0$, the bifurcation diagram is illustrated in Fig. 3. Because the rub-impact rotor system modeled by integer-order damping is addressed adequately in the past, the following analysis is based on $\alpha = 0.5$. The value of s ranges from 0.1 to 4.5 and the step size is 0.003. The vertical axis of Fig. 1 is the non-dimensional X and Y . It is viewed that the system vibration is periodic one motion at very low rotational velocity. Fig. 4 shows the Poincare map, phase trajectory and power spectrum for $s = 0.5$. There is one isolated point in the Poincare map. As the rotating speed increase, the system vibration comes into the periodic two motion region ranging from 1.21 to 1.47. The Poincare map, phase trajectory and power spectrum at $s = 1.3$ is shown in Fig. 5. After undergoing the period motion zone, the rotor system enters into the first chaotic region. Hence the chaotic state remains from 1.53 to 1.90. Fig. 6 shows the rotor orbit, Poincare map and power spectrum for $s = 1.68$. There is a strange attractor representing chaotic motion in the Poincare map and a continuous frequency spectrum in the power spectrum. The corresponding largest Lyapunov exponent when $s = 1.68$ is 0.068. All of these results prove that the system motion is chaotic. At about 1.95, the magnitude skip appears in the sys-

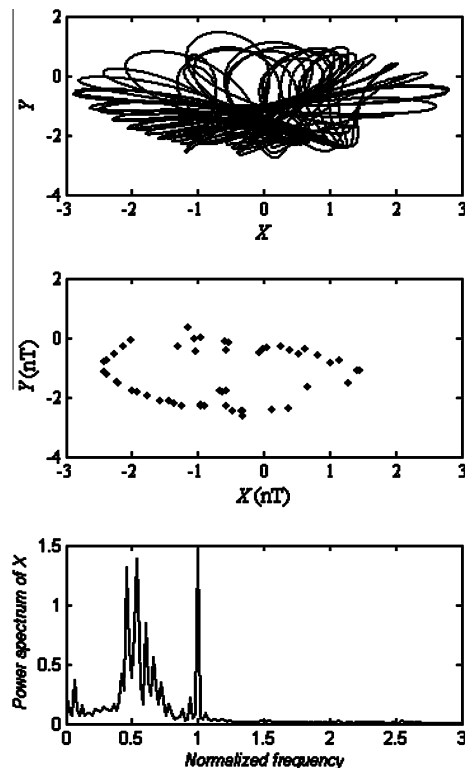


Fig. 11. Phase trajectory, Poincare map and power spectrum for $s = 3.05$.

tem vibration. And then the system comes into the quasi-periodic motion zone remaining from 1.95 to 2.285. Fig. 7 shows the rotor orbit, Poincare map and power spectrum for $s = 2.1$. Irregular rotor orbit and a closed circle in the projection of Poincare section are observed. In order to clearly identify system dynamic behavior from a quantitative view of point, the largest Lyapunov exponent is introduced to support the characteristics of system behavior. The corresponding largest Lyapunov exponent at $s = 2.1$ is 0.

When the speed continues to increase, the system motion comes into the second chaotic region through a route of period doubling bifurcation and leaves chaos through a route of sudden transition from the chaotic to the periodic motion. Fig. 8 shows two points in the Poincare map and two peaks, at $1\times$ and $0.5\times$, in the power spectrum. The periodic four motion at $s = 2.53$ can be illustrated as Fig. 9. Only four points appear in the Poincare map, and there are $1\times$, $0.5\times$, $0.25\times$ and $0.75\times$ in the power spectrum. As the speed increases, the rotor response becomes quasi-periodic, with a closed circle in the Poincare map in Fig. 10. After undergoing quasi-periodic zone, the half frequency motion gradually dominates the rotor response, and the system becomes unstable and suddenly enters into the chaotic motion along with the rubbing. Chaotic motion at $s = 3.05$ is shown in Fig. 11. The irregular orbit, the continuous spectrum with many frequencies, and a great number of discrete points with irregular form appear. Moreover, the corresponding largest Lyapunov exponent is 1.9673. As s further increased, the system vibration response suddenly leaves the chaotic motion and comes into the periodic motion. The periodic two motion exists in the region of $3.79 < s < 4.5$. It can be identified from Fig. 1.

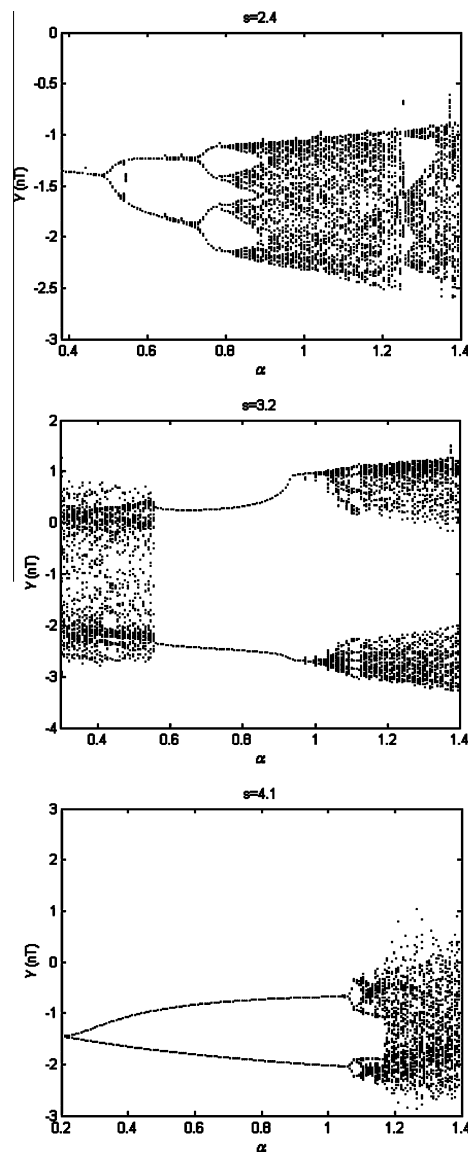


Fig. 12. Bifurcation diagrams of Y versus α : (a) $s = 2.4$, (b) $s = 3.2$, (c) $s = 4.1$.

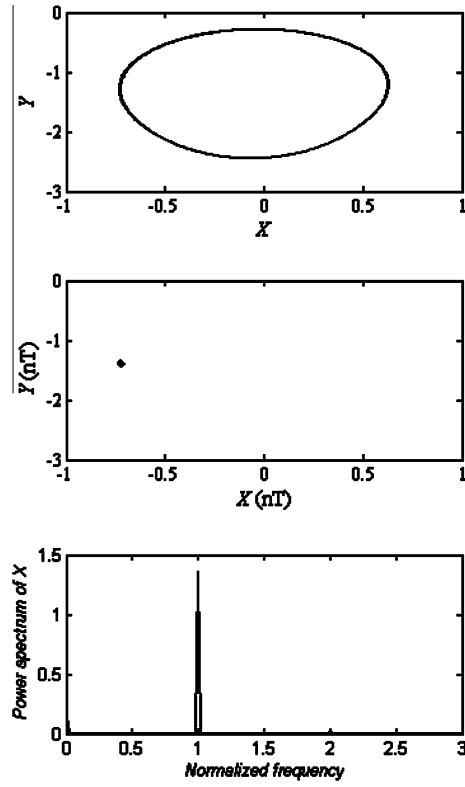


Fig. 13. Phase trajectory, Poincaré map and power spectrum for $\alpha = 0.45$.

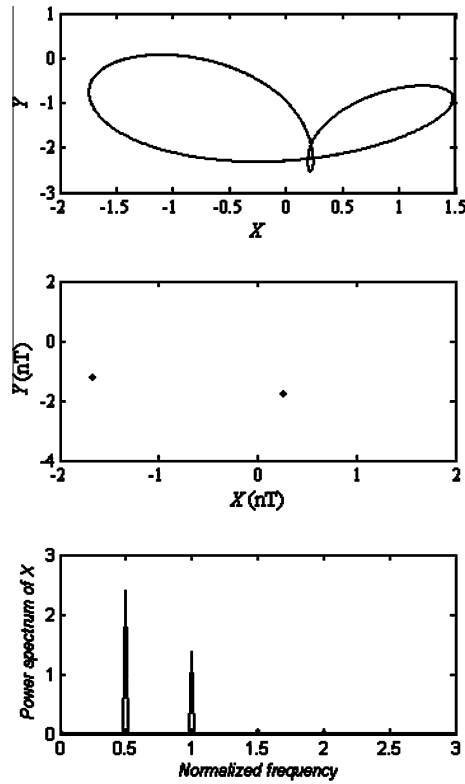


Fig. 14. Phase trajectory, Poincaré map and power spectrum for $\alpha = 0.6$.

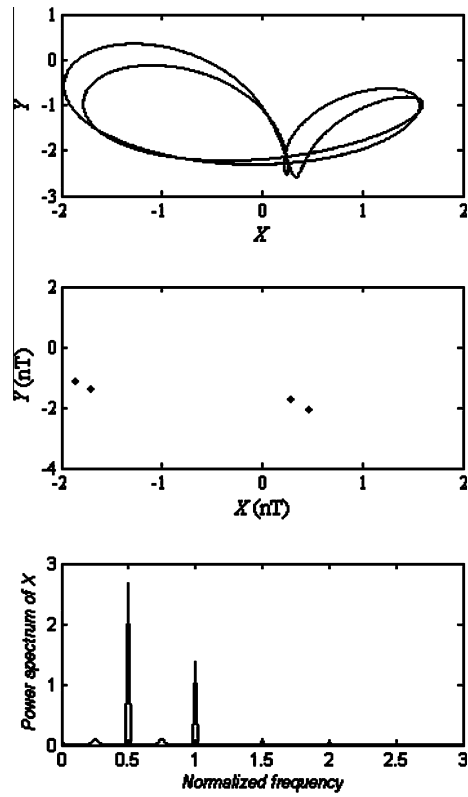


Fig. 15. Phase trajectory, Poincaré map and power spectrum for $\alpha = 0.76$.

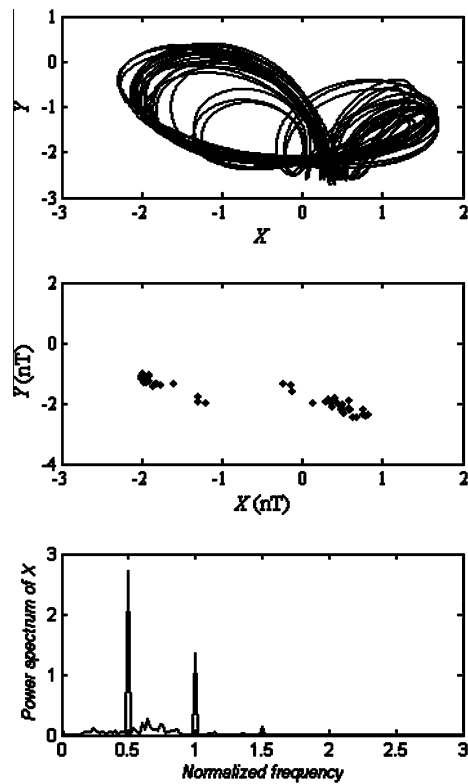


Fig. 16. Phase trajectory, Poincaré map and power spectrum for $\alpha = 1.15$.

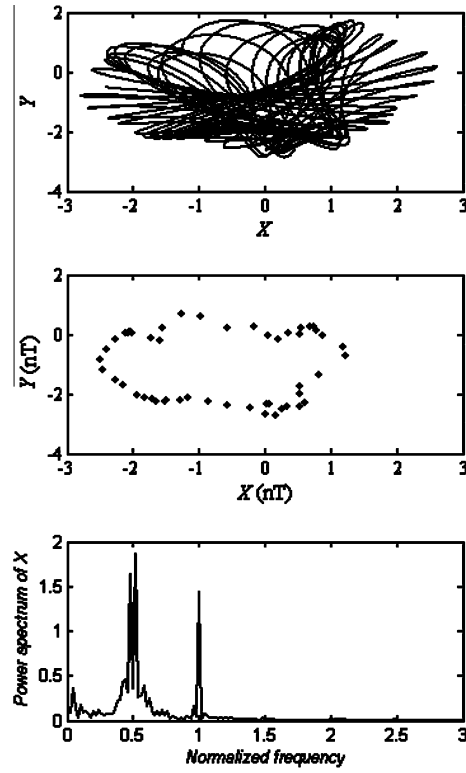


Fig. 17. Phase trajectory, Poincaré map and power spectrum for $\alpha = 0.45$.

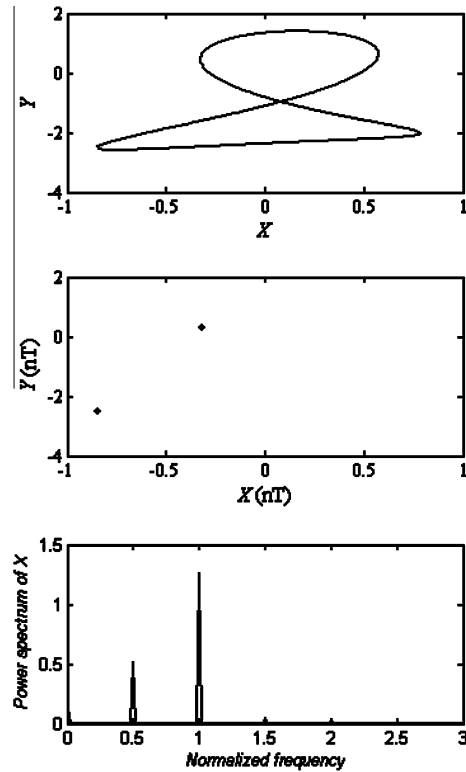


Fig. 18. Phase trajectory, Poincaré map and power spectrum for $\alpha = 0.8$.

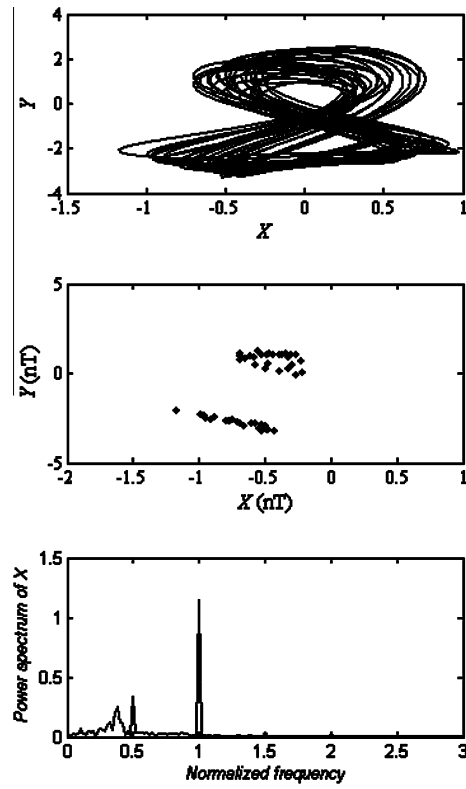


Fig. 19. Phase trajectory, Poincaré map and power spectrum for $\alpha = 1.35$.

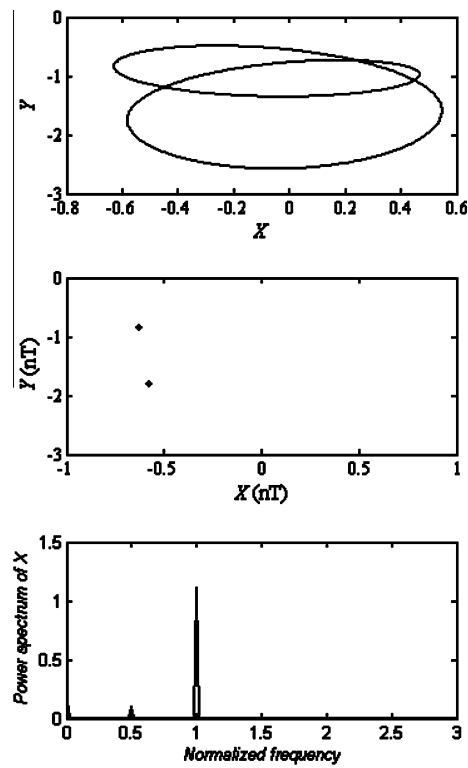


Fig. 20. Phase trajectory, Poincaré map and power spectrum for $\alpha = 0.6$.

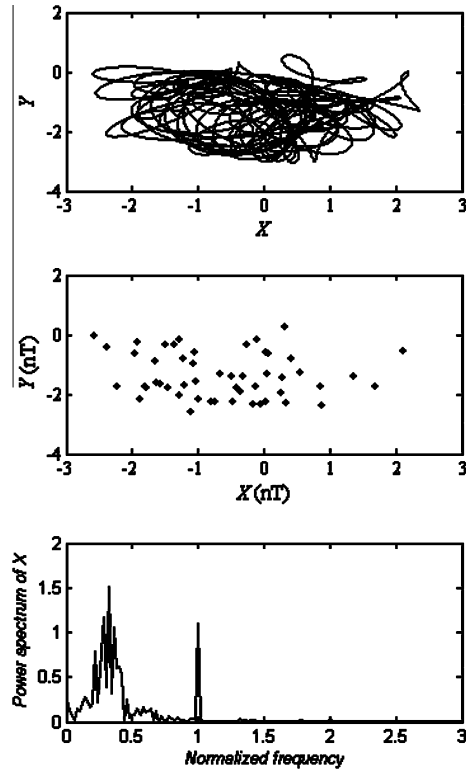


Fig. 21. Phase trajectory, Poincaré map and power spectrum for $\alpha = 1.3$.

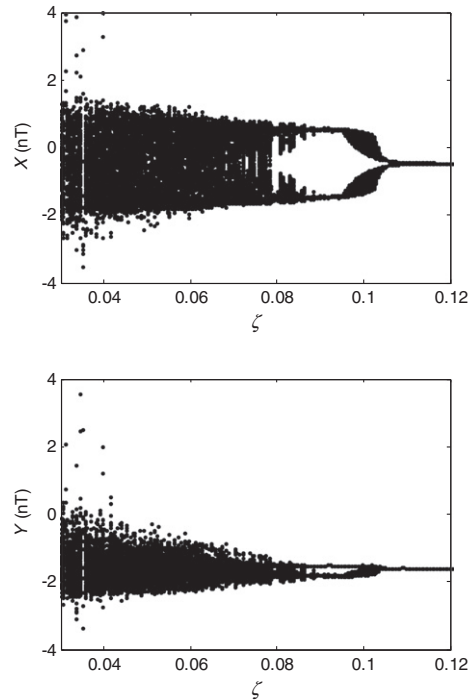


Fig. 22. Bifurcation diagrams of X and Y versus ζ for $s = 2.3$, $\alpha = 0.5$, $\beta = 0.3$.

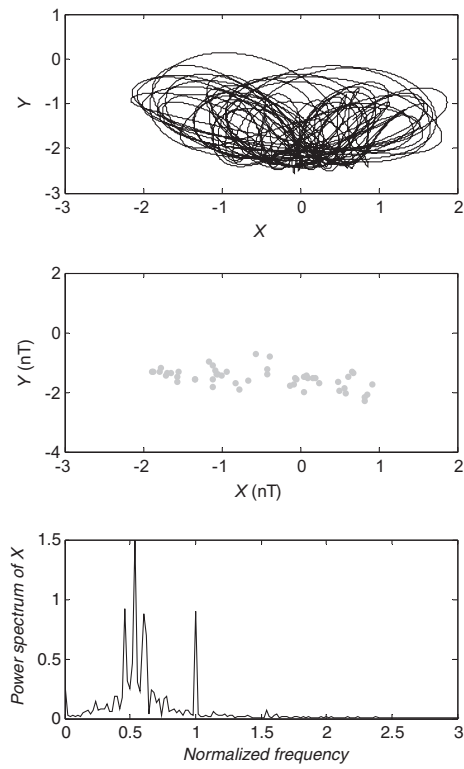


Fig. 23. Phase trajectory, Poincare map and power spectrum for $\zeta = 0.04$, $s = 2.3$.

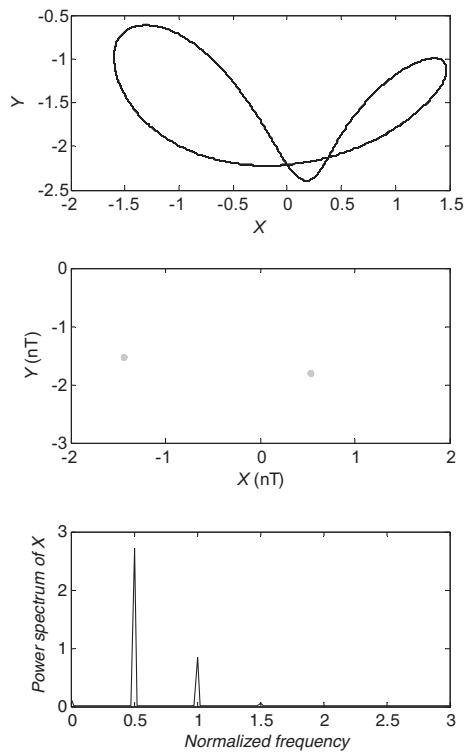


Fig. 24. Phase trajectory, Poincare map and power spectrum for $\zeta = 0.09$, $s = 2.3$.

4.2. Influence of fractional order of damping

The change of dynamic characteristics of rotating machinery is well achieved through damping adjustment. So it is essential to study the effect of the fractional order of damping in order to comprehensively understand the dynamic behavior of fractional rotor system. In the following numerical analysis, the derivative order of damping is used as control parameters of bifurcation diagrams. The range of α is from 0.4 to 1.4, and the step size is 0.007. Fig. 12 shows the vibration response of rub-impact rotor is varying along with the change of α . It can be seen from Fig. 12 that the fractional order exhibits great effect on the dynamic characteristics.

In Fig. 12a, it is obvious that at $s = 2.4$, the rotor response enters into the chaotic zone through the period doubling bifurcation. When $\alpha < 0.49$, the motion is synchronous with periodic one, as demonstrated in Fig. 13. As the fractional order increases, the rotor response becomes synchronous with periodic two for $0.49 < \alpha < 0.72$. Fig. 14 shows that there are two points in the Poincare map and two peaks, at $0.5\times$ and $1\times$, in the power spectrum. From 0.73 to 0.78, the system response becomes periodic four motion as Fig. 15. After undergoing the period doubling bifurcation, the rotor motion comes into the chaotic zone. The motion remains chaotic for $\alpha > 0.89$, as shown in Fig. 16.

In Fig. 12b, it can be observed that at $s = 3.2$, the rotor response leaves the chaotic zone through the route of sudden transition from the chaotic to the periodic two motion, and comes into the second chaotic through the route of period doubling bifurcation. When $0.4 < \alpha < 0.56$, the motion is chaotic, as demonstrated in Fig. 17. There are irregular rotor orbit and the corresponding largest Lyapunov exponent for this case is 0.625. The amplitude of $0.48\times$ is larger than that of $1\times$ in the power spectrum. It can be viewed that the aggravated half frequency motion increases the vibration response and induces the rubbing. As the fractional order increases, the rotor response suddenly becomes synchronous with periodic two for $0.56 < \alpha < 0.97$. Fig. 18 shows two points in the Poincare map and two peaks, at $0.5\times$ and $1\times$, in the power spectrum. After undergoing the period doubling bifurcation, the rotor motion comes into the second chaotic zone. The motion remains chaotic for $1.1 < \alpha < 1.4$, as shown in Fig. 19. There are continuous frequencies in the power spectrum, and two sections of many separated points in Poincare map. The corresponding largest Lyapunov exponent for $\alpha = 1.35$ is 0.7249.

In Fig. 12c, it can be viewed that at $s = 4.1$, the rotor response comes into the chaotic region through the route of period doubling bifurcation. When $0.4 < \alpha < 1.06$, the motion is periodic two with synchronous frequency $1\times$ and sub-synchronous frequency $0.5\times$, as demonstrated in Fig. 20. As the fractional order increases, the rotor response gradually becomes chaotic after undergoing the period doubling bifurcation. The motion maintains chaos from 1.17 to 1.4. Fig. 21 shows the rotor orbit, Poincare map and power spectrum for $\alpha = 1.3$. The corresponding largest Lyapunov exponent for this case is 1.381. In addition,

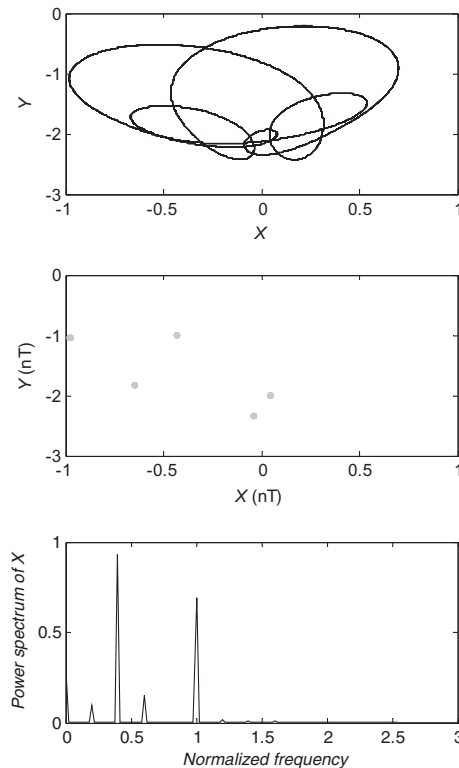


Fig. 25. Phase trajectory, Poincare map and power spectrum for $\zeta = 0.04$, $s = 2.8$.

tion, the irregular rotor orbit, continuous frequency spectrum and a large amount of points in the Poincare map are viewed. All of these results in this case show that the rotor motion is chaotic.

Therefore, we can conclude by the foregoing analysis that the fractional rub-impact rotor system exhibits rich dynamic characteristics. The fractional order of damping has great effect on the dynamic behavior of rotor system. So it can be taken into account in the design and control of rotor-bearing system. Similarly, the value of damping factor is also one of the important parameters affecting the dynamic characteristics of rotor systems. In order to investigate the influence of the va-

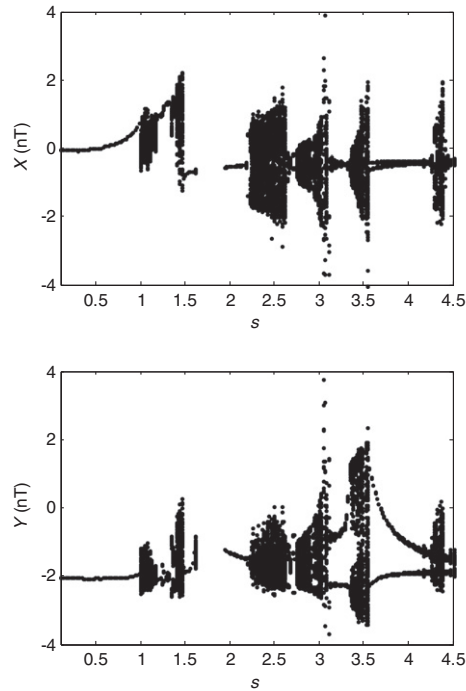


Fig. 26. Bifurcation diagrams of X and Y versus s for $\zeta = 0.06$, $\alpha = 0.5$, $\beta = 0.3$.

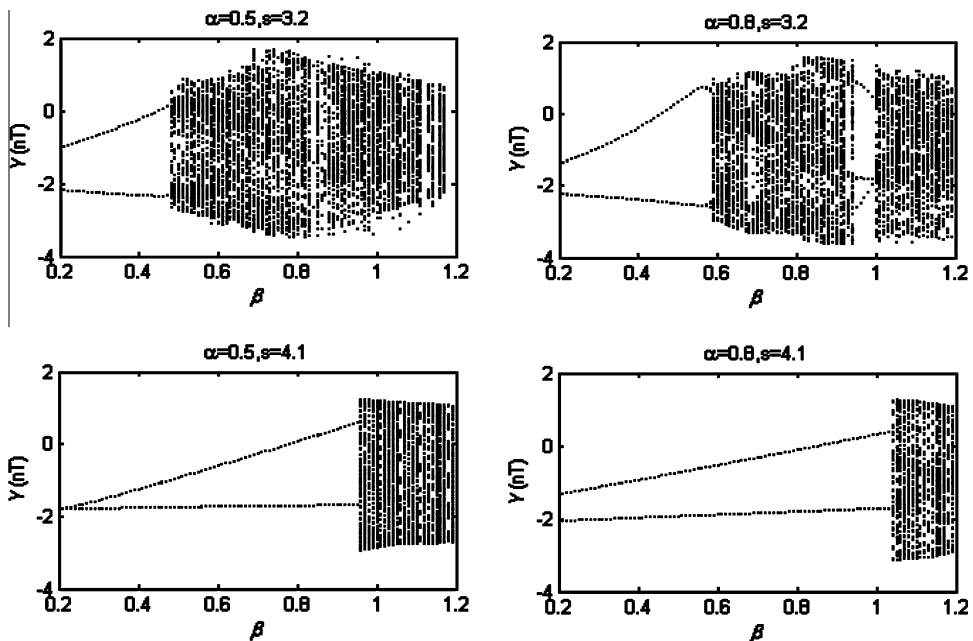


Fig. 27. Bifurcation diagrams of Y versus β .

lue of damping factor, the bifurcation diagram for $0.03 \leq \zeta \leq 0.12$ with step size $\Delta\zeta = 0.0005$ is illustrated in Fig. 22. The other parameters for this case are $\alpha = 0.5$, $s = 2.3$, $\beta = 0.3$. It can be seen from Fig. 22 that as the damping factor increases from 0.03 to 0.12, the rotor system response leaves chaos by the route of inverse period doubling bifurcation and gradually enters into the periodic one motion. Fig. 23 shows the rotor orbit, Poincare map and power spectrum for $\zeta = 0.04$, $s = 2.3$, $\beta = 0.3$. There are irregular rotor orbit and the corresponding largest Lyapunov exponent for this case is 0.486. The amplitude of $0.5\times$ is larger than that of $1\times$ in the power spectrum. It can be viewed that the aggravated half frequency motion increases the vibration response and induces the rubbing. As the damping ratio increases, the rotor response gradually becomes synchronous with periodic two for $0.08 < \zeta < 0.105$, as demonstrated in Fig. 24. There are two points in the Poincare map and two peaks, at $0.5\times$ and $1\times$, in the power spectrum. After undergoing the period doubling bifurcation, the rotor motion comes into the periodic one motion. Fig. 25 shows the rotor orbit, Poincare map and power spectrum for $\zeta = 0.04$, $s = 2.8$, $\beta = 0.3$. There are five points in the Poincare map and five peaks in the power spectrum. When $\zeta = 0.06$, the bifurcation diagram using the speed ratio as the control parameter is shown in Fig. 26. The speed ratio ranges from 0.1 to 4.5 with $\Delta s = 0.02$, the other parameters for this case are $\zeta = 0.06$, $\alpha = 0.5$, $\beta = 0.3$. The much rich dynamic behaviors could be observed through the same methods in Section 4.1.

It is proved by the above analysis that the damping factor is also one of the important parameters affecting dynamic characteristics of rotor system.

4.3. Influence of eccentricity

The exciting forces induced by the mass imbalance are major source of rotor vibrations in field, so it is necessary to analyze the effect of eccentricity on the motion characteristics of the rub-impact rotor system with fractional order damping. Fig. 27 shows bifurcation diagrams for system using β as the control parameter. The range of β is from 0.2 to 1.2, and the step is 0.01. The speed ratio is equal to 3.2 or 4.1. The derivative order of damping is set to 0.5 or 0.8. The other parameters in the numerical simulation for this case are constant.

In Fig. 27, it can be observed that as the mass eccentricity increases, all the system responses at various conditions come into the chaotic state. The main reason is that the increased unbalanced force and vibration amplitude eventually lead to the occurrence of rotor–stator rubbing. The motion becomes chaotic, and this chaos is retained for higher mass eccentricity. Fig. 28 shows the rotor orbit, Poincare map and power spectrum for $s = 3.2$, $\alpha = 0.5$, $\beta = 0.8$. There are irregular rotor orbit, continuous frequency spectrum and a large amount of dispersed points in the Poincare map. The corresponding largest

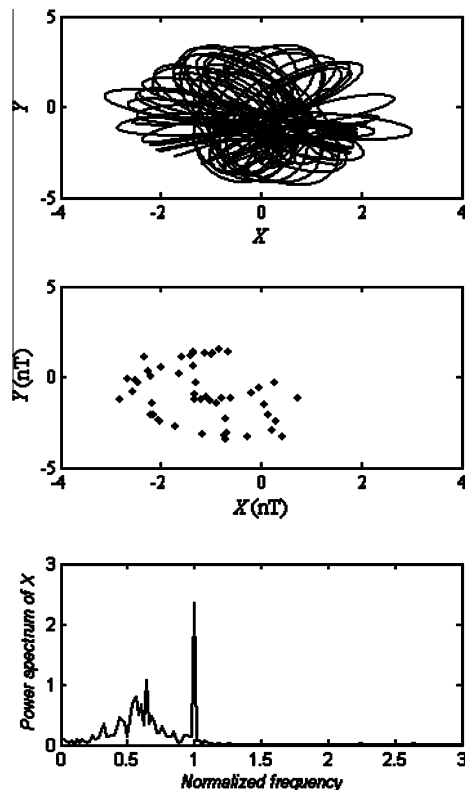


Fig. 28. Phase trajectory, Poincare map and power spectrum for $s = 3.2$, $\alpha = 0.5$, $\beta = 0.8$.

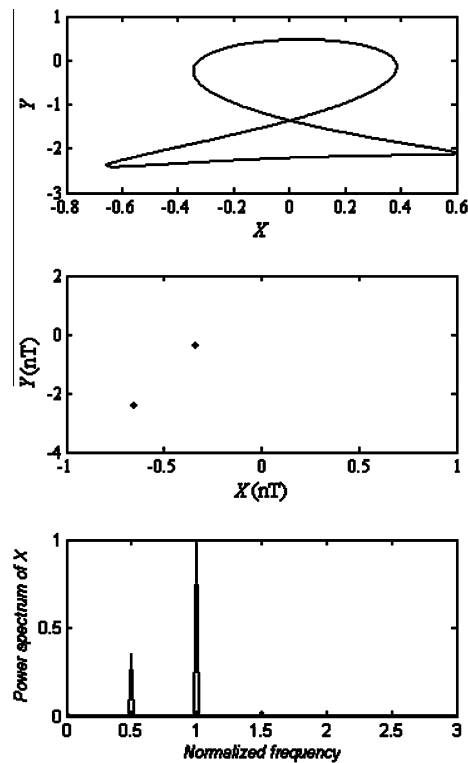


Fig. 29. Phase trajectory, Poincaré map and power spectrum for $s = 3.2$, $\alpha = 0.8$, $\beta = 0.4$.

Lyapunov exponent for this case is 1.015. They can prove the motion is chaotic. While the small mass eccentricity exists, the rotor response is described by Fig. 29. The parameters for this case are $s = 3.2$, $\alpha = 0.8$, $\beta = 0.4$. Only two points in the Poincaré map and two peaks in the power spectrum are examined. Therefore the system response is periodic two motion.

5. Conclusion

The nonlinear dynamics of the fractionally damped rub-impact rotor system are investigated in this paper. The damping model for rub-impact rotor system is described using fractional calculus. A radial elastic force and a tangential Coulomb friction force are assembled to model the rotor–stator rubbing. The four order Runge–Kutta method and ten order CFE–Euler approximation method are used to simulate the fractional order rotor equations.

The phase diagram, Poincaré diagram, bifurcation diagram and the largest Lyapunov exponent are introduced to evaluate the effect of the fractional order, rotating speed and mass eccentricity on dynamic behaviors. The analysis results show that the fractional order damped rotor system exhibits periodic motion, chaos and quasi-periodic motion. A period doubling route to chaos and inverse period doubling route from chaos to periodic motion, sudden transition and quasi-periodic from periodic motion to chaos have appeared clearly.

The numerical results mainly investigate the nonlinear dynamics of rub-impact rotor system with fractional order damping and confirm the significant effect of fractional order on system dynamics. Therefore, more attention should be paid to the fractional order of damping for the design, analysis and control of system dynamics. The next work requires more efforts to prove that the consideration of fractional order damping can improve the results as they are closer to the experimental observations. Furthermore, the experimental validation is essential before any concrete conclusions are drawn for using the fractional order damping for further vibration control.

Acknowledgments

This project jointly support in part by the National Natural Science Foundation of China (Grant Nos. 50805113, 50905113), Important National Science & Technology Specific Projects (Grant No. 2009ZX04014-015) and China Postdoctoral Science Foundation (Grant No. 20080441173). The authors would also like to thank all the reviewers for their comments and suggestions, which are vital for improving the quality of this paper.

References

- [1] Debnath L. Recent applications of fractional calculus to science and engineering. *Int J Math Math Sci* 2003;54:3413–42.
- [2] Sabatier J, Agrawal OP, Tenreiro Machado JA. *Advances in fractional calculus-theoretical developments and applications in physics and engineering*. Berlin: Springer; 2007.
- [3] Padovan J, Sawicki JT. Nonlinear vibrations of fractionally damped systems. *Nonlinear Dyn* 1998;16:321–36.
- [4] JiuHong Jia, XiaoYao Shen, HongXing Hua. Viscoelastic behavior analysis and application of the fractional derivative maxwell model. *J Vib Control* 2007;13(4):385–401.
- [5] Shokooh A, Suárez L. A comparison of numerical methods applied to a fractional model of damping materials. *J Vib Control* 1999;5:331–54.
- [6] Sorrentino S, Fasana A. Finite element analysis of vibrating linear systems with fractional derivative viscoelastic models. *J Sound Vib* 2007;299:839–53.
- [7] Galucio AC, Deu JF, Ohayon R. A fractional derivative viscoelastic model for hybrid active–passive damping treatments in time domain – Application to sandwich beams. *J Intell Mater Syst Struct* 2005;16(1):33–45.
- [8] Borowiec M, Litak G, Syta A. Vibration of the Duffing oscillator: effect of fractional damping. *Shock Vib* 2007;14:29–36.
- [9] Mahmood A, Parveen S, Ara A, Khan NA. Exact analytic solutions for the unsteady flow of a non-Newtonian fluid between two cylinders with fractional derivative model. *Commun Nonlinear Sci Numer Simul* 2009;14(8):3309–19.
- [10] Barbosa RS, Tenreiro Machado JA. Describing function analysis of systems with impacts and backlash. *Nonlinear Dyn* 2002;29:235–50.
- [11] Barbosa RS, Tenreiro Machado JA, Ferreira IM. Describing function analysis of mechanical systems with nonlinear friction and backlash phenomena. In: *IHMNLCO3-2nd IFAC workshop on Lagrangian and Hamiltonian methods for non linear control*, 3–5 April 2003, Sevilla, Spain; 2003. p. 299–304.
- [12] Ge ZM, Jhuang WR. Chaos, control and synchronization of a fractional order rotational mechanical system with a centrifugal governor. *Chaos, Solitons Fractals* 2007;33:270–89.
- [13] Tenreiro Machado JA, Galhano A. Fractional dynamics: a statistical perspective. *ASME J Comput Nonlinear Dyn* 2008;3(2):1–5.
- [14] Muszynska A. Rotor-to-stationary element rub-related vibration phenomenon in rotating machinery – Literature survey. *Shock Vib Digest* 1989;21:3–11.
- [15] Beatty RF. Differentiating rotor response due to radial rubbing. *ASME J Vib Acoust Stress Reliab Design* 1985;107:151–60.
- [16] Chu F, Zhang Z. Bifurcation and chaos in rub-impact Jeffcott rotor system. *J Sound Vib* 1998;210(1):1–18.
- [17] Chu F, Lu W. Experimental observation of nonlinear vibrations in a rub-impact rotor system. *J Sound Vib* 2005;283:621–43.
- [18] Ehrich FF. Some observations of chaotic vibration phenomena in high-speed rotor dynamics. *ASME J Vib Acoust* 1991;113:50–7.
- [19] Goldman P, Muszynska A. Chaotic behavior of rotor/stator systems with rubs. *Trans ASME J Eng Gas Turbine Power* 1994;116:692–701.
- [20] Lin F, Schoen MP, Korde UA. Numerical investigation with rub-related vibration in rotating machinery. *J Vib Control* 2001;7:833–48.
- [21] Feng ZC, Zhang X. Rubbing phenomena in rotor–stator contact. *Chaos, Solitons Fractals* 2002;14(2):257–67.
- [22] Choi YS. Nonlinear parameter identification of partial rotor rub based on experiment. *KSME Int J* 2004;18(11):1969–77.
- [23] Chang-jian CW, Chen CK. Non-linear dynamic analysis of rub-impact rotor supported by turbulent journal bearings with non-linear suspension. *Int J Mech Sci* 2008;50(6):1090–113.
- [24] Qin WY, Chen GR, Meng G. Nonlinear responses of a rub-impact overhung rotor. *Chaos, Solitons Fractals* 2004;19(5):1161–72.
- [25] Shen XY, Jia JH, Zhao M. Numerical analysis of a rub-impact rotor-bearing system with mass unbalance. *J Vib Control* 2007;13(12):1819–34.
- [26] Patel TH, Darpe AK. Vibration response of a cracked rotor in presence of rotor–stator rub. *J Sound Vib* 2008;317(3–5):841–65.
- [27] Podlubny I. *Fractional differential equations*. San Diego: Academic Press; 1999.
- [28] Chen YQ, Moore KL. Discretization schemes for fractional-order differentiators and integrators. *IEEE Trans Circ Syst* 2002;49(3):363–7.
- [29] Valerio D, Costa JS. Time-domain implementation of fractional order controllers. *IEE Proc – Control Theory Appl* 2005;152(5):539–52.
- [30] Ma C, Hori Y. The time-scaled trapezoidal integration rule for discrete fractional order controllers. *Nonlinear Dyn* 2004;38:171–80.
- [31] Tenreiro Machado JA. Fractional derivatives: probability interpretation and frequency response of rational approximations. *Commun Nonlinear Sci Numer Simul* 2009;14(9–10):3492–7.
- [32] Jia JH, Shen XY, Hua HX. Viscoelastic behavior analysis and application of the fractional derivative Maxwell model. *J Vib Control* 2007;13(4):385–401.
- [33] Shokooh A, Suarez L. A comparison of numerical methods applied to a fractional model of damping materials. *J Vib Control* 1999;5(3):331–54.
- [34] Maia NMM, Silva JMM, Ribeiro AMR. On a general model for damping. *J Sound Vib* 1998;218(5):749–67.